Analysis of Radio Frequency and Stability Performance on Double-Gate Extended Source Tunneling Field-Effect Transistors

Saeid Marjani and Seyed Ebrahim Hosseini*
Department of Electrical Engineering
Ferdowsi University of Mashhad
Mashhad, Iran
saeid.marjani@stu.um.ac.ir
*ehosseini@um.ac.ir

***Abstract*— The radio frequency (RF) and stability performance of double-gate (DG) extended source tunneling field-effect transistors (TFETs) are evaluated by extracting RF parameters like cut-off frequency (f_t), maximum oscillation frequency (f_{max}) and stability factor. In addition, the superb RF performances of double-gate extended source TFETs were obtained by designing gate length. The stability factor and small signal parameters such as gate capacitance and transconductance can be extracted using a non-quasi static small signal model are calculated using *Y*-parameters from a TCAD simulation. It was confirmed that the double-gate extended source TFET is suitable for RF applications.**

Keywords*— Radio frequency (RF); Stability factor; Nonquasistatic (NQS); Extended source; Tunneling field-effect transistor (TFET).

I. INTRODUCTION

The tunneling field-effect transistors (TFETs) are one of the promising devices that can achieve a steep sub-threshold slope (SS) of below 60 mV/decade at 300 K of temperature, and can potentially realize low standby power (LSTP) devices at significantly reduced the operating voltage and power dissipation. TFETs, which are reverse biased gated p^+-i-n^+ diodes with heavily doped source and drain regions whose on-current arise due to field-effect controlled band-to-band tunneling (BTBT), have the lower leakage current, suppressed short channel effects (SCE), low standby power consumption and low gate capacitance compared to MOSFETs [1–3].

When the N-type device is off, the source valence band is located below the channel conduction band. Therefore, the presence of large tunneling barrier keeps the off-current extremely low due to the reverse biased operation. When the device is turned on, the energy bands down and the channel conduction band goes below the source valence band. Hence, high lateral electric field forces the electrons to tunnel through the narrow tunneling barrier of source-channel junction [1].

There has been a lot of research interest on the design, modeling, fabrication, and characterization of TFETs [4–22]. However, because silicon-based TFETs have the low on-current due to the low interband tunneling, the on-current of TFETs must be improved. On the other hand, the low on-current causes low transconductance and RF performances. The on-current of TFETs can improve by applying band-gap engineering [8, 9], small band-gap materials [10], high-k dielectric materials [11, 12], pocket doping [13], extended source [7, 14– 16], vertical direction tunneling [17] and p-n-p-n structure [18].

In this work, we investigate a DG extended source TFETs for high performances. By changing the values of the gate length (L_G), the extended source TFETs are designed for RF application. We have obtained RF, small signal and stability factor parameters from the analytical equations of the *Y*-parameters of a nonquasistatic (NQS) radio frequency model. The *Y*-parameters of extended source TFETs having different gate length were evaluated by two-dimensional device simulator simulation using activating multiple physical models for higher accuracy such as nonlocal band-to-band tunneling model, auger recombination, trap assisted tunneling model, band-gap narrowing, Shockley-Read-Hall recombination model, hurkx recombination model and; concentration and field dependent mobility models.

The paper is organized as follows. In section II, we have described the device structure, *Y*-parameters of nonquasistatic equivalent circuit model and stability model of extended source TFETs. The results and discussion are presented in section III. We finally discuss validation of the radio frequency model in section IV, before concluding the paper in section V.

II. DEVICE STRUCTURE AND MODELING

Fig. 1 shows a structure of DG extended source TFET. The doping concentrations of Si-channel, source and drain are p^- 1×10^{15} cm^{-3}, p^+ 1×10^{20} cm^{-3} and n^+ 1×10^{20} cm^{-3}, respectively. The oxide thickness is 2 nm. The channel length of structure is 30 nm, and silicon body thickness, extended source length and nm extended source thickness are 15 nm, 10 nm and 5nm, respectively.

As mentioned in [14], the extended source TFET with short extended source length increases tunneling junction area in the

on-state. Therefore, the increase in tunneling junction area leads to higher BTBT generation rate and boosts on-current. This explains the large improvement in the I_{ON}/I_{OFF} ratio (more than 11 orders of magnitude) because the difference between off-current of the square-shaped extended source and conventional TFET is less pronounced, that is one advantage of the extended source TFET. In order to better clarity about the physics reason for this large improvement, the energy band diagram along the source-drain direction at the oxide-silicon interface (horizontal cut-line) and along the top gate-bottom gate direction at 5 nm away from the source-drain interface (vertical cut-line) are plotted in Fig. 2 for off-state and on-state of extended source TFET.

On the one hand, in off-state, the source valence band is located below the channel conduction band for horizontal and vertical cut-lines of structure. Therefore, the small off-current flows in structure due to the large tunneling barrier in between the source and channel. Consequently, the difference in off-current of extended source and conventional TFET is negligible as mentioned in [14]. But on the other hand, by looking at the energy band diagrams for on-state, the square-shaped extended source TFET has an additional vertical tunneling component as compared conventional TFET where the channel conduction band goes below the square-shaped extended source valence band due to applied gate voltage as observed in Fig. 2 (b). This vertical tunneling component causes the electrons tunnel from the occupied valence band states of the square-shaped extended source to the unoccupied conduction-band states of the channel through the narrow tunneling barrier between the square-shaped extended source and the channel. Consequently, the on-current only increases as compared with the conventional TFET due to the larger tunneling junction area in the on-state introduced by the extended source.

The *Y*-parameters of the intrinsic nonquasistatic small signal equivalent circuit after by considering the assumptions $\omega^2 R_g^2 (C_{gs}+C_{gd})^2 << 1$ and $\omega^2\tau^2 << 1$ are considered as [19],

$$Y_{11} \approx \omega^2 R_g (C_{gs}+C_{gd})^2 + j\omega(C_{gs}+C_{gd}) \quad (1)$$

$$Y_{12} \approx -\omega^2 R_g C_{gd}(C_{gs}+C_{gd}) - j\omega C_{gd} \quad (2)$$

$$Y_{21} \approx g_m - \omega^2 R_g (C_{gs}+C_{gd})(C_{gd}+\tau g_m) - j\omega[C_{gd}+\tau g_m + g_m R_g (C_{gs}+C_{gd})] \quad (3)$$

$$Y_{22} \approx g_{ds} + \omega^2 R_g C_{gd}\{C_{gd} + g_m[\tau + R_g(C_{gs}+C_{gd})]\} + j\omega[C_{gd}+C_{sd}+R_g g_m C_{gd}] \quad (4)$$

where, R_g is the effective gate resistance. C_{gs}, and C_{gd} and C_{sd} are intrinsic gate-source, gate-drain and source-drain capacitance, respectively. Time constant τ, g_m and g_{ds} are the charge transport delay, transconductance and source-drain conductance, respectively.

By using the real and imaginary parts of *Y*-parameters, we obtain the analytical values of the device small signal parameters as [19],

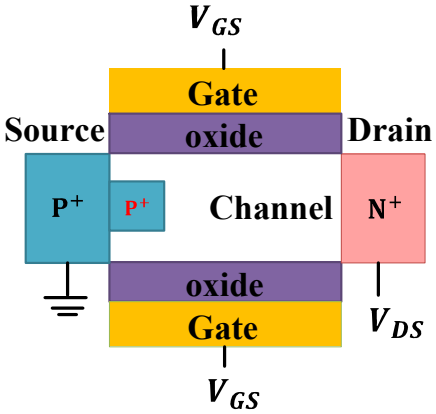

Fig. 1. A structure of the extended source TFET.

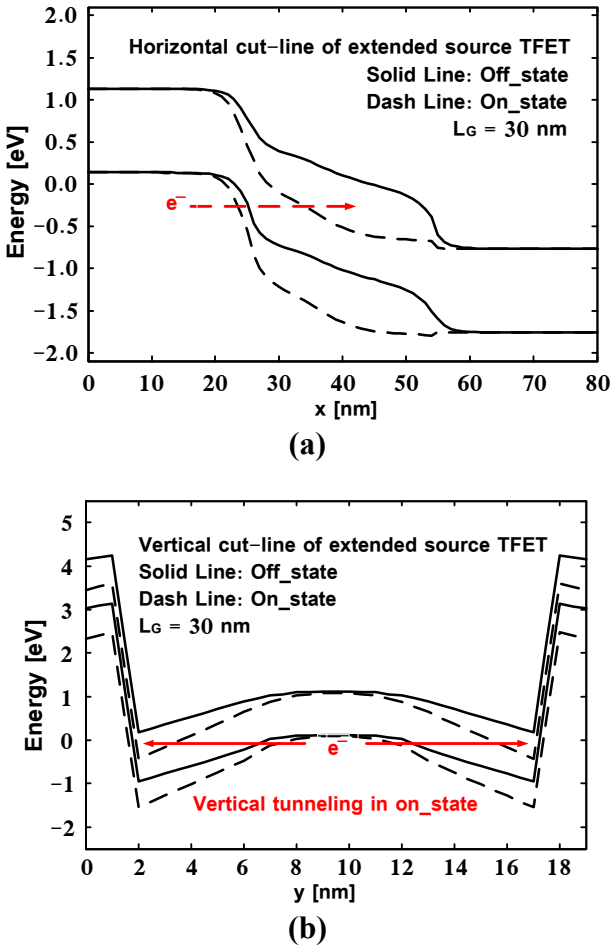

Fig. 2. The energy band diagrams of 30 nm gate length extended source TFET. (a): along the horizontal direction near the oxide-silicon interface (horizontal cut-line). (b): along the vertical direction at 5 nm away from the

$$R_g = \frac{\mathrm{Re}[Y_{11}]}{(\mathrm{Im}[Y_{11}])^2} \quad (5)$$

$$C_{gs} = \frac{\mathrm{Im}[Y_{11}]+\mathrm{Im}[Y_{12}]}{\omega} \quad (6)$$

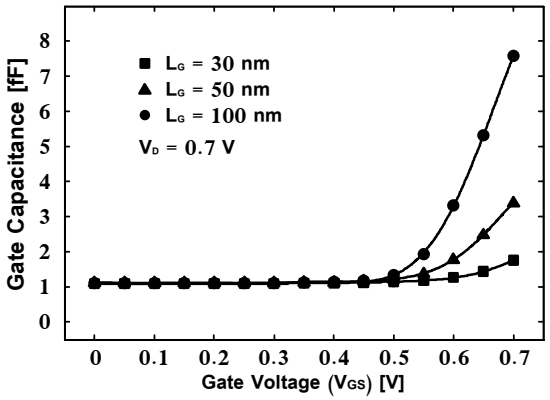

Fig. 3. The gate capacitance of extended source TFETs having L_G = 30, 50 and 100 nm.

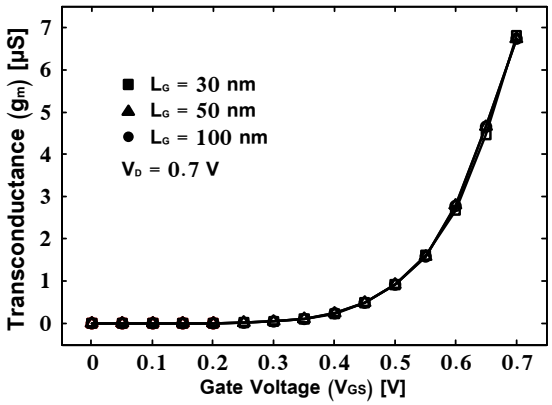

Fig. 4. The transconductance (g_m) of extended source TFETs having L_G = 30, 50 and 100 nm.

$$C_{gd} = -\frac{\mathrm{Im}[Y_{12}]}{\omega} \tag{7}$$

$$C_{sd} = \frac{\mathrm{Im}[Y_{22}]}{\omega} - C_{gd} - R_g g_m C_{gd} \tag{8}$$

$$\tau = -\frac{\frac{\mathrm{Im}[Y_{12}]}{\omega} + C_{dg} + g_m R_g (C_{gs} + C_{gd})}{g_m} \tag{9}$$

$$g_m = \mathrm{Re}[Y_{21}]\big|_{\omega^2=0} \tag{10}$$

$$g_{ds} = \mathrm{Re}[Y_{22}]\big|_{\omega^2=0} \tag{11}$$

Extracted intrinsic small signal parameters using the *Y*-parameters from a TCAD simulation have been used for the evaluation of the RF performances at necessary bias conditions applied to the gate and drain terminals. In order to understand the device behavior at high frequencies, the radio frequency and stability performance of extended source TFET is evaluated by extracting the stability performance, cut-off and maximum oscillation frequencies, known as figures of merit (FoM). The cut-off and maximum oscillation frequencies can be calculated by the current and unilateral power gains using the *Y*-parameters from a TCAD simulation, respectively. Here, cut-off frequency (f_T) is obtained when the current gain is unity ($\left|\frac{Y_{21}}{Y_{11}}\right| = 1$); and maximum oscillation frequency is obtained under power matching condition at the input and output ports (Mason's unilateral power gain) drops to unity [20].

The stability factor (k) determines the stability of a TFET which describes the instable oscillations due to input or output impedance of the transistor. On the other hand, the stability factor gives an indication, whether a TFET is conditionally or unconditionally stable. However, the transistor is conditionally stable at operating frequency below critical frequency but it can oscillate under certain conditions. At any operating frequency above a critical frequency (f_k), TFET is unconditionally stable that the TFET will not begin to oscillate independently. The unconditionally stable condition of TFET is $k > 1$.

The stability factor in terms of *Y*-parameter at different frequencies of operation for the TFET can be expressed as [21],

$$k = \frac{2\,\mathrm{Re}(Y_{11})\,\mathrm{Re}(Y_{22}) - \mathrm{Re}(Y_{12}Y_{21})}{|Y_{12}Y_{21}|} \tag{12}$$

In order to simplify further, by substituting the *Y*-parameters into (12), will yield the stability factor expression (13) as a function of the small signal parameters which is shown at the bottom of the page, where,

$$C_{gg} = C_{gs} + C_{gd} \tag{14}$$

III. Results and Discussion

Fig. 3 shows gate capacitance (C_{gg}) of the extended source TFETs having different gate lengths. The gate capacitance of TFETs is more affected by the influence of the gate-drain capacitance at high gate voltage (V_{GS}). Due to the reduction of potential barrier at the drain side with the increase in V_{GS}, the gate-drain capacitance increases. Therefore, the values of gate capacitance are increased when the gate voltage is applied. As seen, the 30 nm extended source TFET has beenpotential as RF device with low gate capacitance.

The Fig. 4 shows the transconductances (g_m) of extended source TFETs having L_G = 30, 50 and 100 nm. Since the drain current (I_D) of TFET is not affected by gate length, there is no change in transconductances of TFETs with different gate lengths, as shown in Fig. 4.

Fig.5 shows cut-off (f_T) and maximum oscillation frequencies (f_{max}) of extended source TFETs for different gate length values as a function of V_{GS}. The value of cut-off

$$k = \frac{\omega^2(C_{gd}^{\ 2} + 2C_{gg}(C_{gs}g_{ds} + C_{gd}(g_{ds} + g_m))R_g + C_{gd}g_m\tau + C_{gd}C_{gg}^{\ 2}R_g^{\ 2}(C_{gd} + 2C_{gd}g_mR_g + g_m(2C_{gs}R_g + \tau))\omega^2)}{\sqrt{(g_m^{\ 2} + (C_{gd} + g_m\tau)^2\omega^2)(C_{gd}\omega + C_{gd}C_{gg}^{\ 2}R_g^{\ 2}\omega^3)^2}} \tag{13}$$

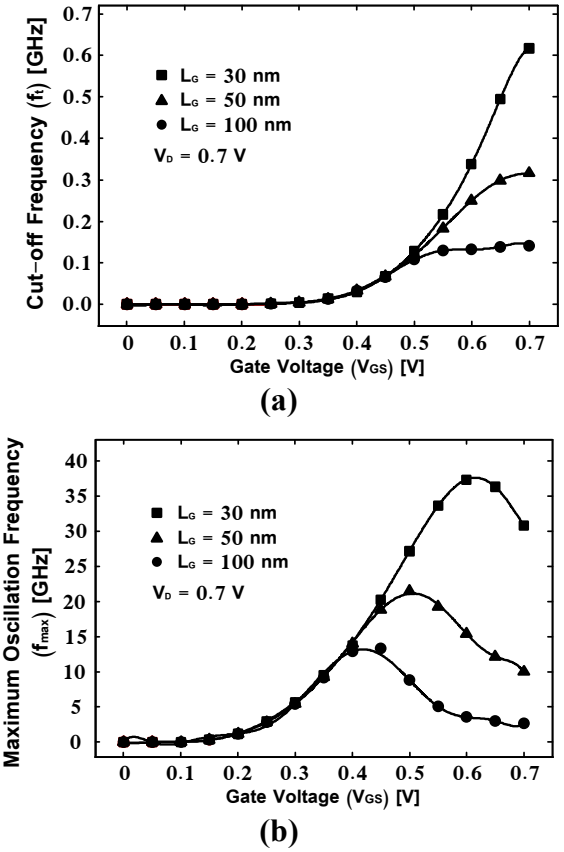

Fig. 5. (a) The f_T and (b) f_{max} of extended source TFETs having L_G = 30, 50 and 100 nm as a function of V_{GS}.

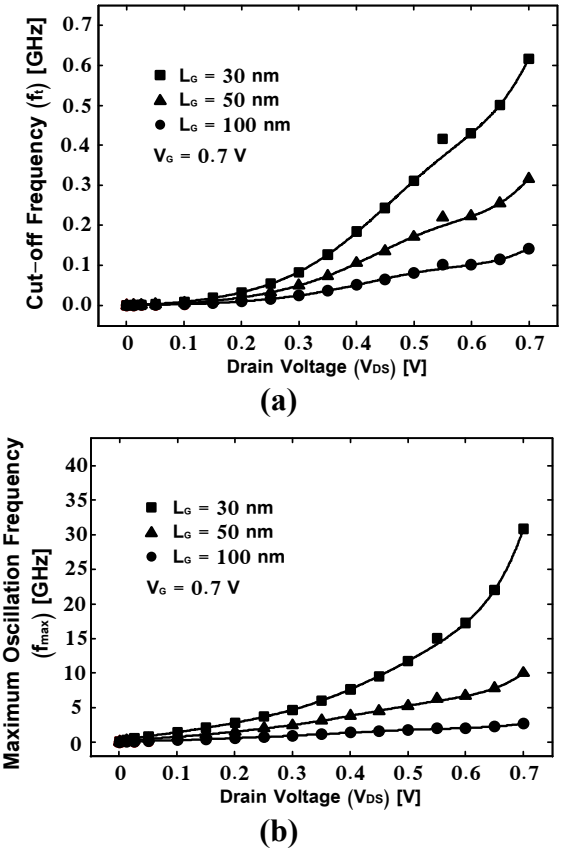

Fig. 6. (a) The f_T and (b) f_{max} of extended source TFETs having L_G = 30, 50 and 100 nm as a function of V_{DS}.

frequency is increased with the increase of V_{GS} by the relation between the transconductance and gate capacitance ($f_T \sim \frac{g_m}{2\pi \times C_{gg}}$). The cut-off frequency of a TFET is inversely proportional to gate length. Because C_{gg} is proportional to gate length and the transconductance of a TFET is nearly constant. The f_T of TFETs have the rising tendency as a function of V_{GS} since g_m and C_{gg} increase monotonically with the increase of V_{GS} as shown in Figs. 3 and 4. As seen from Fig.5 that 30 nm extended source TFET shows a better f_T as well as f_{max} compared to other lengths at high V_{GS}. It should be mainly due to the lower gate capacitance as shown in Fig. 3; however, its transconductance is nearly similar to other TFETs. Furthermore, the extended source TFET with 30 nm gate length has higher f_{max} values than other TFETs because of higher f_T and lower C_{gg} as previously shown in Figs. 4 and 5(a).

Fig. 6 shows f_T and f_{max} of extended source TFETs having L_G = 30, 50 and 100 nm as a function of V_{DS}. Due to the improvement in the drain current [22], the transconductance rapidly increases as V_{DS} increases. It can be seen from Fig. 6(a), the cut-off frequency increases. The TFET shows higher the f_{max} due to the higher cut-off frequency and lower gate capacitance at higher V_{DS}, as shown in Fig. 6(b). It can be seen that the 30 nm extended source TFET exhibits the better RF performances because of the higher transconductance and current drivability at high V_{DS}.

Fig. 7 demonstrates the stability factor extended source TFETs for different gate length values up to 250 GHz. The critical frequency (f_k) values of the extended source with 30, 50 and 100 nm gate lengths were about 28.1, 9.3 and 2.7 GHz at V_{GS} = V_{DS} = 0.7 V, respectively. Consequently, the additional stability circuits are not required for RF circuits above these frequencies. The reduction in gate length leads to increase in short-channel effect and has the impact on stability performance of TFET.

The results indicate that 30 nm extended source TFETs can have higher cut-off and maximum oscillation frequencies for high efficiency switching applications with good stability.

IV. Validation of Radio Frequency Model

Fig. 8 compares the modeled and simulated values of small signal parameters such as capacitances and effective gate resistance for a 30 nm extended source TFET as a function of the frequency at V_{GS} = V_{DS} = 0.7 V up to 250 GHz. It is observed that small signal parameters obtained from the model show excellent agreement with the calculation results by the TCAD simulation.

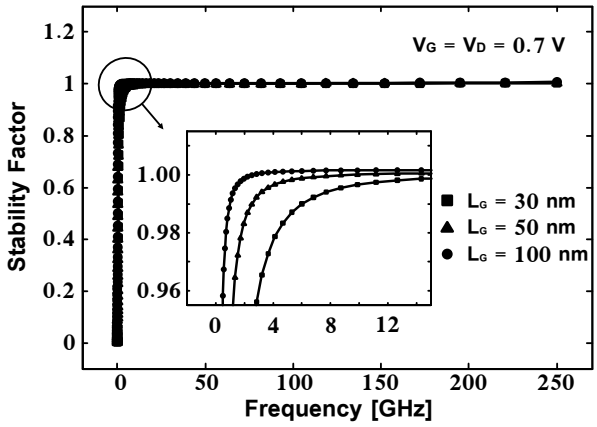

Fig. 7. The stability factor extended source TFETs having L_G = 30, 50 and 100 nm.

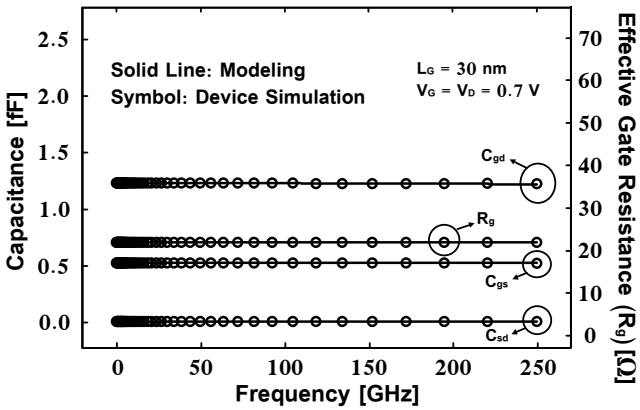

Fig. 8. Comparison of modeled and simulated of capacitances and effective gate resistance a 30 nm extended source TFET.

V. CONCLUSION

The RF and stability characteristics of DG extended source TFETs are performed through parameter extractions from the model equivalent circuit in terms of the cut-off frequency, maximum oscillation frequency and stability factor. Furthermore, the device stability is studied for various gate lengths. The optimized gate length shows excellent stability performance with optimal cut-off frequency. Since the device is unconditionally stable from 2.7 GHz, there is no need of any additional stabilization network above this critical frequency. The device has shown improved RF performance and circuit complexity that suitable for RF applications.

REFERENCES

[1] A. M. Ionescu and H. Riel, "Tunnel field-effect transistors as energy-efficient electronic switches," Nature, Vol. 479, No. 7373, pp. 329-337, 2011.

[2] B. Ghosh and M. W. Akram, "Junctionless tunnel field effect transistor," IEEE Electron Device Lett., Vol. 34, No. 5, pp. 584-586, 2013.

[3] B. Rajamohanan, D. Mohata, A. Ali, S. Datta, "Insight into the output characteristics of III-V tunneling field effect transistors," J. Appl. Phys., Vol. 102, pp. 092105-1–092105-5, 2013.

[4] A. Vallett, S. Minassian, P. Kaszuba, S. Datta, J. Redwing and T. Mayer, "Fabrication and characterization of axially doped silicon nanowire tunnel field-effect transistors," Nano let., Vol. 10, No. 10, pp. 4813-4818, 2010.

[5] G. Dewey, B. Chu-Kung, J. Boardman, JM. Fastenau, J. Kavalieros, WK. Liu, D. Lubyshev, M. Metz, N. Mukherjee, P. Oakey, R. Pillarisetty, M. Radosavljevic, HW. Then and R. Chau, "Fabrication, characterization, and physics of III–V heterojunction tunneling field effect transistors (H-TFET) for steep subthreshold swing", in IEEE international electron device meeting (IEDM), Washington, DC, USA, pp. 5-7, 2011.

[6] M. Gholizadeh and S. E. Hosseini, "A 2-D analytical model for double-gate tunnel FETs," IEEE Trans. Electron Devices, Vol. 61, No. 5, pp. 1494-1500, 2014.

[7] S. Marjani and S. E. Hosseini, "Radio-frequency modeling of square-shaped extended source tunneling field-effect transistors," Superlattices and Microstructures, Vol. 76, pp. 297-314, 2014.

[8] L. Britnell, R. V. Gorbachev, R. Jalil, B. D. Belle, F. Schedin, A. Mishchenko, T. Georgiou, M. I. Katsnelson, L. Eaves, S. V. Morozov, N. M. R. Peres, J. Leist, A. K. Geim, K. S. Novoselov, L. A. Ponomarenko, "Field-effect tunneling transistor based on vertical graphene heterostructures," Science, Vol. 335, No. 6071, pp. 947-950, 2012.

[9] S. Richter, C. Sandow, A. Nichau, S. Trellenkamp, M. Schmidt, R. Luptak, K. K. Bourdelle, Q. T. Zhao, and S. Mantl, "Ω-Gated silicon and strained silicon nanowire array tunneling FETs," IEEE Electron Device Lett., Vol. 33, No. 11, pp. 1535-1537, 2012.

[10] K-T. Lam, X. Cao, and J. Guo, "Device Performance of Heterojunction Tunneling Field-Effect Transistors Based on Transition Metal Dichalcogenide Monolayer," IEEE Electron Device Lett., Vol. 34, No. 10, pp. 1331-1333, 2013.

[11] K. Boucart and A. M. Ionescu, "Double-gate tunnel FET with high-k gate dielectric," IEEE Trans. Electron Devices, Vol. 54, No. 7, pp. 1725-1733, 2007.

[12] A. Mallik and A. Chattopadhyay, "Tunnel field-effect transistors for analog/mixed signal system-on-chip applications," IEEE Trans. Electron Devices, Vol. 59, No. 4, pp. 888-894, 2012.

[13] K. Kao, A. S. Verhulst, W. G. Vandenberghe and K. De Meyer, "Counterdoped pocket thickness optimization of gate-on-source-only tunnel FETs," IEEE Trans. Electron Devices, Vol. 60, No. 1, pp. 6-12, 2013.

[14] Y. Yang, P. Guo, G. Han, K. L. Low, C. Zhan and Y.-C. Yeo, "Simulation of tunneling field-effect transistors with extended source structures," J. Appl. Phys., Vol. 111, pp. 114514-1– 114514-8, 2012.

[15] G. B. Beneventi, E. Gnani, A. Gnudi, S. Reggiani and G. Baccarani, "Dual-metal-gate InAs tunnel FET with enhanced turn-on steepness and high on-current," IEEE Trans. Electron Devices, Vol. 61, No. 3, pp. 776-784, 2014.

[16] S. Marjani and S. E. Hosseini, "A novel double gate tunnel field effect transistor with 9 mV/dec average subthreshold slope," in 22st Iranian Conference on Electrical Engineering (ICEE), Tehran, Iran, pp. 399-402, 2014.

[17] L. Lattanzio, N. Dagtekin, L. D. Michielis and A. M. Ionescu, "On the static and dynamic behavior of the germanium electron-hole bilayer tunnel FET" IEEE Trans. Electron Devices, Vol. 59, No. 11, pp. 2932-2938, 2012.

[18] S. Marjani and S. E. Hosseini, "RF modeling of p-n-p-n double-gate tunneling field-effect transistors," presented at the 3rd Conference on Millimeter-Wave and Terahertz Technologies (MMWaTT), Tehran, Iran, 2014.

[19] I. Kwon, M. Je, K. Lee and H. Shin, "A simple and analytical parameter-extraction method of a microwave MOSFET," IEEE Trans. Microwave Theory Tech., Vol. 50, No. 6, pp. 1503-1509, 2002.

[20] V. Dimitrov, J. Heng, K. Timp, O. Dimauro, R. Chan, M. Hafez, J. Feng, T. Sorsch, W. Mansfield, J. Miner, A. Kornblit, F. Klemens, J. Bower, R. Cirelli, E. J. Ferry, A. Taylor, M. Feng, and G. Timp, "Small-Signal Performance and Modeling of sub-50nm nMOSFETs with fT above 460-GHz," Solid State Electron., Vol. 52, No. 6, pp. 899-908, 2008.

[21] J.M. Rollet, "Stability and power gain invariants of linear two ports," IRE Trans. Circuit Theory, Vol. 9, pp. 29-32, 1962.

[22] S. Cho, J. S. Lee, K. R. Kim, B.-G. Park, J. S. Harris, Jr., and I. M. Kang, "Analyses on small-signal parameters and radio-frequency modeling of gate-all-around tunneling field-effect transistors," IEEE Trans. Electron Devices, Vol. 58, No. 12, pp. 4164-4171, 2011.